Identification of the Nitrogen Split Interstitial $(\text{N-N})_{\text{N}}$ in GaN

H. J. von Bardeleben,[1,*] J. L. Cantin,[1] U. Gerstmann,[2] A. Scholle,[2] S. Greulich-Weber,[2] E. Rauls,[2] M. Landmann,[2] W. G. Schmidt,[2] A. Gentils,[3,4] J. Botsoa,[4] and M. F. Barthe[4]

[1]*INSP, Université Pierre et Marie Curie, UMR 7588 au CNRS 4 place Jussieu, 75005 Paris, France*
[2]*Department Physik, Universität Paderborn, Warburger Strasse 100, 33098 Paderborn, Germany*
[3]*CSNSM, Université Paris-Sud and CNRS-IN2P3, 91405 Orsay Campus, France*
[4]*CNRS/CEMHTI, CNRS UPR 3079/CEMHTI, 1D avenue de la Recherche Scientifique, 45071 Orléans, France*

(Received 21 August 2012; published 16 November 2012)

Combining electron paramagnetic resonance, density functional theory, and positron annihilation spectroscopy (PAS), we identify the nitrogen interstitial defect in GaN. The isolated interstitial is unstable and transforms into a split interstitial configuration $(\text{N-N})_{\text{N}}$. It is generated by particle irradiation with an introduction rate of a primary defect, pins the Fermi level at $E_C - 1.0$ eV for high fluences, and anneals out at 400 °C. The associated defect, the nitrogen vacancy, is observed by PAS only in the initial stage of irradiation.

DOI: 10.1103/PhysRevLett.109.206402 PACS numbers: 71.55.Eq, 71.15.−m, 76.30.Mi, 78.70.Bj

Gallium nitride is a wideband semiconductor with a multitude of applications in micro- and optoelectronics. Its high cohesive energy imposes particular growth conditions, and as-grown epitaxial film or bulk samples contain a high number of point and extended defects, which influence their electronic and optical properties [1–3]. Contrary to the case of GaAs where most of the native intrinsic defects have been identified and characterized in detail [4], this is not the case for GaN. The nature of the intrinsic defects in GaN is not known with the exception of the Ga interstitial [5–7] and the Ga monovacancy [8]. Numerous other paramagnetic defects have been observed, mainly by optically detected magnetic resonance, but their hyperfine structure was in general not resolved rendering their identification impossible. In particular, experimental results for the defects related to the nitrogen sublattice are missing: the N vacancy has not yet been clearly detected by positron annihilation spectroscopy (PAS) or electron paramagnetic resonance (EPR) and the N interstitial has escaped any detection. As GaN is considered radiation hard as compared to other III–V compounds such as GaAs and GaP, it is of considerable interest to clarify whether low thermal annealing stages of nitrogen sublattice related defects are at the origin of this property.

In this work, we have studied in detail an irradiation-induced, intrinsic defect characterized by an introduction rate of a primary defect. We present its identification by EPR as a N interstitial in a split-interstitial configuration (cf. Fig. 2). Based on density functional theory (DFT) and molecular dynamics calculations [9–11] the model of N split-interstitial defects has been proposed before as the stable configuration of the N interstitial, but up to now no experimental evidence for this defect had been obtained. Its identification in this work is based on EPR measurements and theoretical prediction of the hyperfine structure and the g tensors of the main intrinsic defects in GaN. It should be recalled that intuitive models established in the absence of such calculations have often turned out to be erroneous [8,12,13]. We show that in GaN the situation is also complicated, making the support from detailed model calculations a necessity. We also show by PAS the concurrent formation and room temperature stability of nitrogen and gallium monovacancies.

For the controlled formation of intrinsic defects we have chosen particle irradiation. We have irradiated undoped and 2×10^{18} cm^{-3} Si doped n-type GaN bulk crystals grown by hydride vapor phase epitaxy by different types of particles: high energy (20 MeV) electrons, high-energy protons (12 MeV), and swift heavy Si ions (120 MeV). Fluences of up to $10^{18} e- /\text{cm}^2$, $8 \times 10^{16} p+ /\text{cm}^2$, and $10^{14}\text{Si}+ /\text{cm}^2$ have been applied. Given the sample thickness of 340 μm, a homogeneous defect formation can be expected for such $e-$ and $p+$ irradiation conditions. For example, the simulated projected range for 12 MeV protons, e.g., is 450 μm. We observe by EPR in all three cases the same dominant irradiation-induced paramagnetic defect. As the most detailed results have been obtained for proton irradiation, these results will be presented here in particular.

EPR measurements have been performed with X-band and Q-band spectrometers including *in situ* optical excitations. In addition, high frequency (345 GHz) EPR measurements, decisive for establishing the defect symmetry, have also been performed. The absolute defect concentration has been determined with the help of a spin standard sample (Al_2O_3:Cr). For the room temperature PAS experiments, a fast positron source (^{22}Na) in a conventional fast-fast coincidence spectrometer with a time resolution of 225 ps was used. After subtracting the source and background components, the lifetime spectra $L(t) = \sum_i I_i \exp(-t/\tau_i)$ were fitted using a modified version of the software POSFIT [14]. In the analysis of the PAS results on the

2×10^{18} Si doped samples, the information obtained from the EPR measurements showing a progressive electrical compensation with a Fermi-level shift from initially $E_c -$ 35 meV (Si shallow donor) to $E_c - 1.0$ eV for fluences above $1 \times 10^{16} p + /\text{cm}^2$ has been crucial.

In Fig. 1 (left), we show a typical X-band EPR spectrum observed under thermal equilibrium conditions at $T = 4$ K. It displays a rich, partially resolved HF structure which is best resolved for $B \parallel c$. When measured at Q band the EPR spectrum is unchanged (cf. Fig. 1, left) proving that its structure is due to HF interaction and belongs to one single defect. At Q-band frequencies a weak anisotropy of the center of gravity of the spectrum is observed between $g_{\parallel c} = 2.000$ and $g_{\perp c} = 1.998$, which might indicate an axial C_{3v} symmetry. However, the very high frequency (345 GHz) EPR measurements for B 20° from the c axis (cf. Fig. 1, right) show that the symmetry is lower, C_{1h} or C_1, with a clearly anisotropic g tensor with $\Delta g > 0.01$. The concentration of this defect is very high and increases linearly with dose (Fig. 2) after a threshold fluence of 1×10^{16} cm^{-2}. Calibration with the spin standard sample gives a concentration of 1.3×10^{18} cm^{-3} in the 4×10^{16} cm^{-2} irradiated sample corresponding to an introduction rate of 33 cm^{-1} for 12 MeV protons. The spectrum is photosensitive: under *in situ* photoexcitation at 4 K with a threshold energy of 1.0 eV its intensity is increased, demonstrating that this defect pins the Fermi level at $E_c - (1.0 \pm 0.1)$ eV for fluences above 2×10^{16} cm^{-2}. This observation is in agreement with transport measurements in heavily neutron, proton, or electron irradiated GaN, which showed a Fermi-level pinning close to $E_c - 0.9$ eV [15–17]. Based on its level position, this defect was tentatively attributed to a N interstitial.

In GaN, the attribution of a paramagnetic center to a specific defect model even in the case of resolved HF structure is not straightforward when more than one nucleus is involved. The coexistence of two Ga isotopes with nuclear spin $I = 3/2$ and comparable natural abundance, but different nuclear g factor, ^{69}Ga ($g_N = 1.34439$, 60.1%) and ^{71}Ga ($g_N = 1.70818$, 39.9%) as well as two nitrogen isotopes ^{15}N, ^{14}N render the analysis difficult. Most often, multiple HF interactions lead generally to broad lines without resolved HF structure. But even when the HF structure is resolved, detailed calculations are required for their assignment. For this reason we have calculated the defect structures as well as the spectroscopic signatures for the main intrinsic defects from first principles within DFT. We use supercells containing up to 324 atoms, standard norm-conserving pseudopotentials, a plane-wave basis with an energy cutoff of 90 Ryd (Ga 3d electrons in the valence [18]), and the spin-polarized Perdew-Burke-Ernzerhof (PBE) [19] functional. All defect structures have been fully relaxed using $2 \times 2 \times 2$ Monkhorst-Pack k-point samplings. The EPR parameters are calculated taking into account relativistic effects. Whereas the HF splittings are determined by the magnetisation density $m(\vec{r})$ in a very small region around the nuclei [20], the deviation of the g tensor from the free-electron value 2.002319 is driven by spin-orbit coupling as mediated by the spin currents $\vec{j}(\vec{r})$ induced by the external magnetic field [21]. To calculate these characteristic deviations $\Delta g_{\mu\nu}$, we use the gauge-including projector augmented plane wave approach [22] as implemented in the QUANTUM-ESPRESSO package [23]. Note that at least $4 \times 4 \times 4$ k-point samplings are necessary to obtain well-converged elements of the electronic g tensor.

As shown in Fig. 3, the low temperature EPR spectrum for $B \parallel c$ can be well simulated by the parameters

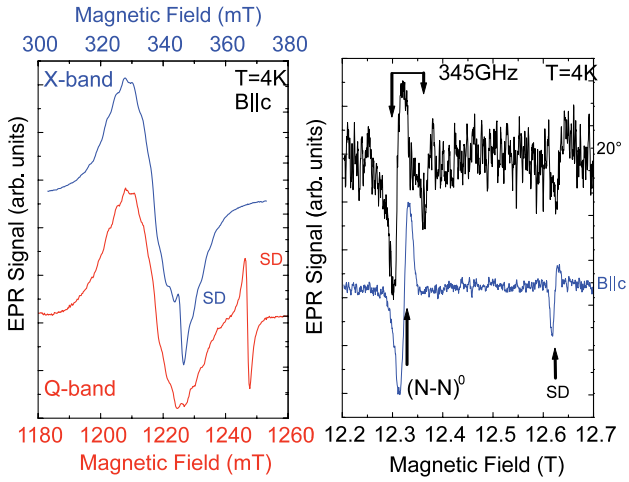

FIG. 1 (color online). Left: X-band (blue, top) and Q-band (red, bottom) EPR spectrum at $T = 4$ K of the $(\text{N-N})_\text{N}$ center and the shallow donor (SD) center for $B \parallel c$. Right: High frequency spectra (345 Ghz) for $B \parallel c$ and 20° from the hexagonal c axis, $T = 4$ K.

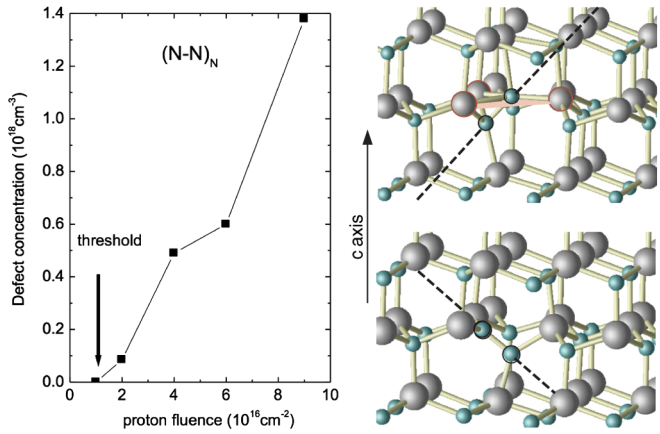

FIG. 2 (color online). Left: $(\text{N-N})_\text{N}$ defect concentration as a function of $p+$ fluence. Right: Ground state (bottom) and excited configuration (top), where one of the N-N dimer atoms has moved through the plane of the 3 Ga ligands (red). Defect axes (orientation of the N-N dimers, dashed lines) are also given.

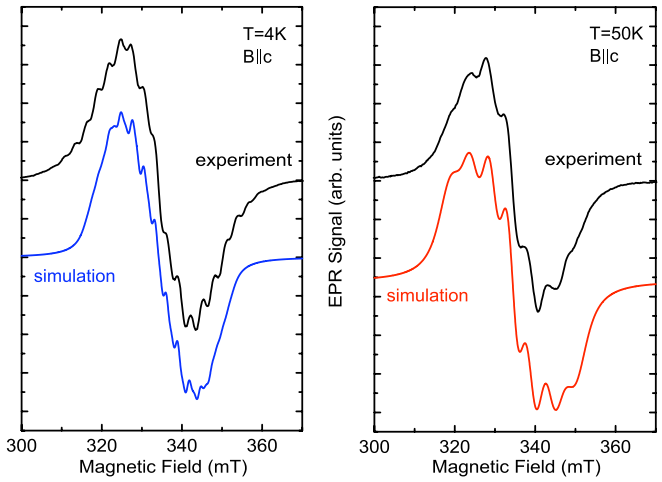

FIG. 3 (color online). X-band EPR spectrum of the $(\text{N-N})_\text{N}$ center at $B \parallel c$ measured at $T = 4$ K (left) and 50 K (right) and the spectra simulated with the values given in Table I.

calculated for the neutral N split interstitial: it is a spin $S = 1/2$ center with C_1 symmetry, a g factor of 2.0016, and a HF interaction with *two* N and *four inequivalent* Ga neighbors (cf. Table I). Its HF structure is similar (magnitude of the splittings) but distinctly different from the previously observed $L1$ center. Based on the assignment of its HF stucture to three Ga neighbors, it had been attributed to a gallium vacancy [6]. The $L1$ center is not observed in our samples, nor any spectrum related to Ga interstitials [5–7]. The calculated g values and HF interactions for the isolated V_Ga, the $V_\text{Ga}V_\text{N}$ divacancy, and also for the $V_\text{Ga}\text{O}_\text{N}$ pairs all give similar results but do not correspond to those of our measured spectrum.

In order to further confirm its *neutral* charge state, we have calculated the energy of the $(\text{N-N})_\text{N}$ charge transitions using the concept of the Slater-Janak transition state [24]. The standard PBE functional leads to values of $E_c - 1.5$ eV $(^{2+/+})$ and $E_c - 0.35$ eV $(^{0/-})$, which both do not agree with the experimental value of -1.0 eV (see Table II). The accuracy of charge transition levels calculated using local functionals like PBE, however, suffers from the well-known DFT band gap problem. To get more reasonable estimates, we performed additional total energy calculations using the nonlocal Heyd-Scuseria-Ernzerhof (HSE) hybrid functional [25] which is known to improve the energetics of defect levels [26]. A range-dependent incorporation of up to 32% Hartree-Fock exact exchange corrects the band gap from 1.89 eV (PBE) to 3.55 eV, close to the experimental value of 3.51 eV [27]. Moreover, the $(^{0/-})$ transition level is shifted considerably: a HSE value of $E_v + 2.54$ eV, 1.01 eV below the conduction band, agrees nicely with the experimental finding.

The HF structure of this defect is temperature dependent (cf. Fig. 3): for $T > 50$ K it changes and the spectrum becomes isotropic with a resolved structure for all orientations of the applied field. The EPR spectrum can be observed up to 300 K. It can again be explained by the HF interaction with *two* N and *four* Ga nuclei but with modified HF parameters. A thermally activated reorientation of a defect leading to a change in the HF parameters has often been observed in semiconductors. We have been able to model this new structure in the following way. At 4 K the structure has C_1 symmetry with the unpaired electron mainly localized in the p-like orbitals of the two central N atoms. The resulting magnetization density resembles a four-leaf clover which is tilted with respect to the crystal axes (cf. Fig. 4). For $T > 50$ K the central N atoms start to fluctuate in position, and the clover leaf oscillates with respect to the N-N axis. The resulting thermally averaged structure shows a higher symmetry, C_{1h}, whereby the distance between the two N atoms is reduced. The magnetization density is also reduced and partially transferred to two of the nearest Ga ligands. The result is a modified HF interaction and EPR line shape with a pronounced central structure. It should be noted that a similar EPR spectrum measured at 77 K has been reported very recently by Son *et al.* in electron irradiated GaN [28,29]. It has been tentatively attributed by these authors to a $V_\text{Ga}\text{O}_\text{N}$ center. However, this assignment is not supported by our modeling.

We have investigated the annealing stage by isochronal annealings (30 min) between 100 °C and 400 °C. Even though the electrical compensation changes only slightly after the 400°C treatment (the samples are still highly resistive), we observe a complete annealing of this defect in the 300 °C to 400 °C range. Figure 2 (right) also shows an excited configuration (0.35 eV higher in energy) from which one of the N-N dimer atoms can easily move

TABLE I. Calculated and experimental g tensor and hyperfine tensors $|A|$ [MHz] (^{69}Ga and ^{14}N) of the $(\text{N-N})_\text{N}^{2+}$ split interstitial for $B \parallel c$ and different EPR measuring temperatures.

		$g_\parallel$	A_N1	A_N2	A_Ga1	A_Ga2	$A_\text{Ga3,4}$
V_Ga^{2-}	C_{1h}	2.0051	52			66	70
$(V_\text{Ga}\text{O}_\text{N})^-$	C_{1h}	2.0049	52			67	71
$(V_\text{Ga}V_\text{N})^-$	C_{1h}	2.0059	52			67	71
$(\text{N-N})_\text{N}^{2+}$	C_{1h}	1.9868	15	3		12	82
$(\text{N-N})_\text{N}^0$	C_1	2.0016	25	42	116	82	45/50
Exp. 4 K		2.0000	15	42	117	92	65/75
Exp. 50 K		2.0005	10	30	110	110	<25
$(\text{N-N})_\text{N}^0$	C_{1h}	2.0009	10	18	125	125	20

TABLE II. Charge transition levels of the $(\text{N-N})_\text{N}$ split interstitial [eV] with respect to the conduction band minimum E_c

Functional	$(2+/+)$	$(+/0)$	$(0/-)$	E_gap
PBE	-1.50	-0.72	-0.35	1.89 eV
HSE	-2.56	-1.45	-1.01	3.55 eV
Exp. (this work)			-1.0	3.51 eV

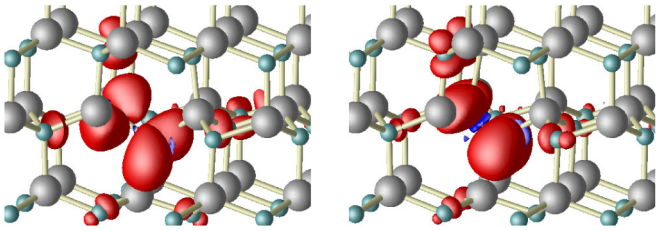

FIG. 4 (color online). Magnetization density (unpaired electron) of the neutral N split interstitial: "symmetry-free" ground state (left) and thermally averaged state with C_{1h} symmetry (right).

through the plane of the three Ga ligands. Hence, this configuration can assist in an efficient *stepwise* N diffusion along the hexagonal channels parallel to the c axis. In SiC, carbon split interstitials $(\text{C-C})_\text{C}$ anneal in the same low temperature range [11]. Their diffusion and rearrangements play an important role in the amorphization process under high fluences of particle irradiation. We expect that N split interstitials play a similar role in GaN.

In n-type and semi-isolating material, the Ga monovacancy will be in the diamagnetic V_Ga^{3-} charge state and is EPR silent. If the Fermi level is pinned at $E_c - 1.0$ eV, the same is true for the N vacancy, which is equally in the diamagnetic V_N^{+} state [3]. PAS spectroscopy is complementary to EPR in the sense that it is not restricted to paramagnetic charge states. It probes neutral and negative vacancies as the V_Ga^{3-}: The average positron lifetime τ_av in our samples increases with the proton fluence (cf. Table III), meaning that the concentration and/or the average size of the vacancy defects increases. Hence, besides an irradiation-induced modification of the electrical compensation, several lifetime compounds must be considered in a detailed analysis of the PAS results. The longest lifetime component τ_3 (235 ± 10 ps) has already been detected by Saarinen *et al.* in GaN [30,31]. It has been convincingly attributed to a V_Ga-related defect which can be either the isolated Ga vacancy or a complex involving V_Ga. Its intensity increases from 35.9% for the lowest fluence to 74.9% for the highest one, indicating that the concentration of the V_Ga-related defects increases with the proton fluence. For the lowest fluence, we observe an additional lifetime component τ_2 of 181 ± 1 ps. This lifetime is clearly shorter than the 235 ps for V_Ga and longer than the bulk value ("as-received" sample), suggesting a second type of vacancy defect; its intensity decreases rapidly with increasing proton fluence. The obvious candidate is the nitrogen vacancy: Tuomisto *et al.* [30] have observed a N-vacancy related lifetime of 180–190 ps in low energy electron irradiated GaN. With increasing fluence of particle irradiation it can be expected to switch from a negative or neutral to a positive charge state [30] becoming, thus, invisible in PAS. The best decomposition of the lifetime spectra, however, is obtained using three lifetime components, one free component and the two others fixed at 190 and 235 ps (cf. Table III). The free component gives short lifetimes between 146 and 154 ps, very close to the bulk value, suggesting that shallow traps are still detected after irradiation.

TABLE III. Experimental positron lifetimes obtained at fluences $\leq 2 \times 10^{16}$ cm^{-2} for an analysis with three lifetime components, one free and two fixed to 190 and 235 ps. In the sample irradiated at 4×10^{16} cm^{-2}, $\tau_\text{av} = 208$ ps is observed.

Fluence	τ_av	τ_1	I_3 [%]	τ_2	I_2 [%]	τ_3	I_3 [%]
As-received		155.3	100.0				
1×10^{15}	187.4	153.4	52.4	190.0	14.4	235.0	33.0
1×10^{16}	191.3	146.4	36.8	190.0	27.2	235.0	36.0
2×10^{16}	200.4	154.2	41.0	190.0	6.0	235.0	53.0

In summary, we report the EPR observation of a nitrogen sublattice defect in GaN which is generated by room temperature particle ($e-$, $p+$, ions) irradiation, the $(\text{N-N})_\text{N}$ split interstitial. It is electrically active and pins the Fermi level 1 eV below the conduction band. The N split interstitial anneals at 400 °C, the first annealing stage for room temperature irradiation. Its high introduction rate and multiple gap levels demonstrate its importance for the electrical compensation under radiation conditions. Our results modify the current understanding of the electrical compensation due to particle irradiation. Whereas previously the compensation between N vacancy donors, N interstitial acceptors, and Ga vacancy acceptors has been considered [32,33], our results show that the N interstitial is ambipolar, i.e., a deep acceptor defect with a level at $E_c - 1.0$ eV in n-type material and a deep donor in p-type material. As its introduction rate is close to the theoretical value for primary N interstitials, the transformation in the split interstitial is apparently complete in n-type and semi-insulating material.

The work was funded by DFG. The calculations have been done at PC^2 (Paderborn) and HLRS (Stuttgart). We thank the Grenoble high field laboratory for the high frequency EPR measurements.

*vonbarde@insp.jussieu.fr

[1] K. Saarinen, T. Suski, I. Grzegory, and D. C. Look, Physica (Amsterdam) B **308–310**, 77 (2001).
[2] F. Tuomisto, T. Paskova, S. Figge, D. Hommel, and B. Monemar, J. Cryst. Growth **300**, 251 (2007).
[3] C. G. van de Walle and J. Neugebauer, J. Appl. Phys. **95**, 3851 (2004).
[4] J. C. Bourgoin, H. J. von Bardeleben, and D. Stievenard, J. Appl. Phys. **64**, R65 (1988).
[5] K. H. Chow, G. D. Watkins, A. Usui, and M. Mizuta, Phys. Rev. Lett. **85**, 2761 (2000).
[6] K. H. Chow, L. Vlasenko, P. Johannesen, C. Bozdog, G. Watkins, A. Usui, H. Sunakawa, C. Sasaoka, and M. Mizuta, Phys. Rev. B **69**, 045207 (2004).

[7] H. Itoh, A. Kawasuso, T. Ohshima, M. Yoshikawa, I. Nashiyama, S. Tanigawa, S. Misawa, H. Okumura, and S. Yoshida, Phys. Status Solidi A **162**, 173 (1997).
[8] K. Saarinen, T. Suski, I. Grzegory, and D. C. Look, Phys. Rev. B **64**, 233201 (2001).
[9] F. Gao, E. J. Bylaska, and W. J. Weber, Phys. Rev. B **70**, 245208 (2004).
[10] H. Y. Xiao, F. Gao, X. T. Zu, and J. Weber, J. Appl. Phys. **103**, 123529 (2008).
[11] H. Y. Xiao, F. Gao, X. T. Zu, and J. Weber, J. Appl. Phys. **105**, 123527 (2009).
[12] B. Aradi, A. Gali, P. Deák, J. Lowther, N. Son, E. Janzén, and W. Choyke, Phys. Rev. B **63**, 245202 (2001).
[13] T. T. Petrenko, T. L. Petrenko, and V. Ya Bratus, J. Phys. Condens. Matter **14**, 12 433 (2002).
[14] P. Kirkegaard and M. Eltrup, Comput. Phys. Commun. **3**, 240 (1972).
[15] D. C. Look, Z. Q. Fang, and B. Claflin, J. Cryst. Growth **281**, 143 (2005).
[16] A. Y. Polyakov *et al.*, J. Appl. Phys. **100**, 093715 (2006).
[17] A. Y. Polyakov, I.-H. Lee, N. B. Smirnov, A. V. Govorkov, E. A. Kozhukhova, N. G. Kolin, A. V. Korulin, V. M. Boiko, and S. J. Pearton, J. Appl. Phys. **109**, 123703 (2011).
[18] U. Gerstmann, A. P. Seitsonen, and F. Mauri, Phys. Status Solidi B **245**, 924 (2008).
[19] J. P. Perdew, K. Burke, and M. Ernzerhof, Phys. Rev. Lett. **78**, 1396 (1997).
[20] P. E. Blöchl, Phys. Rev. B **62**, 6158 (2000).
[21] U. Gerstmann, M. Rohrmüller, F. Mauri, and W. G. Schmidt, Phys. Status Solidi C **7**, 157 (2010).
[22] Ch. J. Pickard and F. Mauri, Phys. Rev. Lett. **88**, 086403 (2002).
[23] P. Giannozzi *et al.*, J. Phys. Condens. Matter **21**, 395502 (2009); http://www.quantum-espresso.org.
[24] S. Sanna, Th. Frauenheim, and U. Gerstmann, Phys. Rev. B **78**, 085201 (2008).
[25] J. Heyd and G. E. Scuseria, J. Chem. Phys. **121**, 1187 (2004).
[26] A. Janotti, J. L. Lyons, and C. G. Van de Walle, Phys. Status Solidi A **209**, 65 (2012).
[27] C. Mietze, M. Landmann, E. Rauls, H. Machhadani, S. Sakr, M. Tchernycheva, F. Julien, W. Schmidt, K. Lischka, and D. As, Phys. Rev. B **83**, 195301 (2011).
[28] N. T. Son, C. Hemmingsson, T. Paskova, K. Evans, A. Usui, N. Morishita, T. Ohshima, J. Isoya, B. Monemar, and E. Janzén, Phys. Rev. B **80**, 153202 (2009).
[29] N. T. Son, C. G Hemmingsson, N. Morishita, T. Ohshima, T. Paskova, K. R. Evans, A. Usui, J. Isoya, B. Monemar, and E. Janzén, Phys. Scr. **T141**, 014015 (2010).
[30] F. Tuomisto, V. Ranki, D. Look, and G. Farlow, Phys. Rev. B **76**, 165207 (2007).
[31] K. Saarinen *et al.*, Physica (Amsterdam) B **273–274**, 33 (1999).
[32] D. C. Look, D. Reynolds, J. Hemsky, J. Sizelove, R. Jones, and R. Molnar, Phys. Rev. Lett. **79**, 2273 (1997).
[33] D. C. Look, G. C. Farlow, P. J. Drevinsky, D. F. Bliss, and J. R. Sizelove *et al.*, Appl. Phys. Lett. **83**, 3525 (2003).